Climate Change Multi-Model Projections in CMIP6 Scenarios in Central Hokkaido, Japan

Shilei Peng
Hokkaido University
Chunying Wang (wangchunying1987@yahoo.com)
North China University of Water Resources and Electric Power
Zhan Li
Hokkaido University
Kunihito Mihara
Hokkaido University
Kanta Kuramochi
Hokkaido University
Yo Toma
Hokkaido University
Ryusuke Hatano
Hokkaido University

Article

Keywords: Ishikari River, climate change, shared socioeconomic pathway-representative concentration pathway scenario, coupled model intercomparison project phase 6, downscaling, statistical downscaling model

Posted Date: March 25th, 2022

DOI: https://doi.org/10.21203/rs.3.rs-1434007/v1

Article

Climate Change Multi-Model Projections in CMIP6 Scenarios in Central Hokkaido, Japan

Shilei Peng [1], Chunying Wang [2*], Zhan Li [3], Kunihito Mihara [1], Kanta Kuramochi [1], Yo Toma [1] and Ryusuke Hatano [1]

[1] Research Faculty of Agriculture, Hokkaido University, Sapporo 0608589, Japan; pengshilei10@gmail.com (S.P.); kmhr@chem.agr.hokudai.ac.jp (K.M.); kanta@chem.agr.hokudai.ac.jp (K.K.); toma@chem.agr.hokudai.ac.jp (Y.T.); hatano@chem.agr.hokudai.ac.jp (R.H.)
[2] North China University of Water Resources and Electric Power, Zhengzhou 450045, China; wangchunying1987@yahoo.com (C.W.)
[3] Graduate School of Science, Hokkaido University, Sapporo 0608589, Japan; blizhan@icloud.com (Z.L.)
* Correspondence: (**Chunying Wang**) email: wangchunying1987@yahoo.com

Abstract: Simulating future climate changes (like temperature and rainfall) is critical for water resource management, disaster mitigation, and agricultural development. Based on the category-wise indicator method, two preferred Global Climate Models (GCMs) for the Ishikari River basin (IRB), the socio-economic center of Hokkaido, Japan, were examined from the newly released Coupled Model Intercomparison Project Phase 6 (CMIP6). Climatic variables (maximum/minimum temperature and precipitation) were projected by the Statistical DownScaling Model (SDSM) under all shared socioeconomic pathway-representative concentration pathway (SSP-RCP) scenarios (SSP1-1.9, SSP1-2.6, SSP2-4.5, SSP3-7.0, SSP4-3.4, SSP4-6.0, SSP5-3.4OS, and SSP5-8.5) in two phases: 2040–2069 (2040s) and 2070–2099 (2070s), with the period of 1985-2014 as the baseline. Predictors of SDSM were derived from CMIP6 GCMs and the reanalysis dataset NOAA-CIRES-DOE 20th Century Reanalysis V3 (20CRv3). Results showed that CMIP6 GCMs had a significant correlation with temperature measurements, but could not represent precipitation features in the IRB. The constructed SDSM could capture the characteristics of temperature and precipitation during the calibration (1985-1999) and validation (2000-2014) phases, respectively. The selected GCMs (MIROC6 and MRI-ESM-2.0) generated higher temperature and less rainfall in the forthcoming phases. The SSP-RCP scenarios had an apparent influence on temperature and precipitation. High-emission scenarios (like SSP5-8.5) would project a higher temperature and lower rainfall than the low-emission scenarios (like SSP1-1.9). Spatial-temporal analysis indicated that the northern part of the IRB is more likely to become warmer with heavier precipitation than the southern part in the future. Higher temperature and lower rainfall were projected during the late 21st century (2070s) than the mid-century (2040s) in the IRB.

Keywords: Ishikari River, climate change, shared socioeconomic pathway-representative concentration pathway scenario, coupled model intercomparison project phase 6, downscaling, statistical downscaling model

Introduction

The current rate and scale of global warming are exceptional with respect to the pre-industrial age[1]. It is increasingly evident that climate change will drive longer and more vigorous-intensity to extremes with severe impacts on humanity[2], economy[3], and natural ecosystems[4]. Limiting global temperature increases to 1.5 °C is vital to staving off the worst warming climate-related risks[5,6]. As a response, it is critical to investigate possible variations in future climatic variables, which should be a major issue for different stakeholders to manage regional catastrophic hazards, prevent significant consequences, as well as establish adaption plans.

Due to the constraints in studies of historical fluctuations and known trends, climate forecasts are required for decision support modeling[7]. The World Climate Research Program (WCRP) Coupled Model Intercomparison Project (CMIP) provides one of the most advanced tools, the Global Climate Model (GCM). GCMs are commonly employed in studies to reproduce physical processes in the atmosphere, ocean, terrestre, and cryosphere. They also provide feedback on global or continental climatic changes under various emission scenarios[8]. The Fourth and Fifth Assessment Reports of the Intergovernmental Panel on Climate Change, IPCC AR4 and AR5, exhibit and evaluate different generations of GCM outputs of CMIP3 and CMIP5[9,10]. However, lots of studies pointed out there are limitations in previous CMIP3- or CMIP5-based GCMs[11,12]. Those products lack of complete information about atmospheric-climatic processes, leading to significant uncertainties and climate sensitivities[13-15]. The latest CMIP6 phase aims to improve the mechanism of emission scenarios and increase the horizontal resolution, making future possibilities more plausible[16,17].

Nevertheless, the performance of GCMs for simulating regional climatic variables still does not satisfy the accuracy requirement of practitioners[18]. Hence, it needs to fabricate local-scale daily climatic conditions by applying a downscaling approach. Statistical downscaling approaches have become a preferred method for inferring regional information from coarse GCMs. They play the role of "bridge" to connect the large scale and local areas[19,20]. Statistical downscaling strategies also have the irreplaceable aspects to provide information that other methodological approaches (e.g., dynamical downscaling) cannot give, even as developing new generation GCMs with higher resolution[19]. The Statistical Downscaling Model (SDSM) is the preferred approach to eliminate errors from GCMs[21].

Lots of SDSM-related studies have demonstrated SDSM's ability to generate future change scenarios[22]. For example, Gebrechorkos et al. (2019) utilized SDSM to draw future temperature and rainfall changes in East Africa (Ethiopia, Kenya, and Tanzania)[23]. Emami and Koch (2019) employed SDSM to reveal the influence of temperature change on water resources in a mountainous area from Iran[24]. Phuong et al. (2020) utilized SDSM to reproduce future climatic variables (precipitation and temperature) on the daily scale under RCP scenarios in a river basin of mid-Vietnam[25]. However, only two common GCMs (CanESM2 and HadCM3) were widely employed to access climatic variables in SDSM. These studies have largely ignored the assessment of GCMs adaptability to reduce the uncertainty and GCM selection in specific study locations. A rigorous evaluation of GCMs before they are applied in hydrology or agricultural management might boost

stakeholders' confidence in using GCMs[26]. Wilby and Harris (2006) created a probabilistic approach to overcome CMIP3 GCM conflicts about regional climatic changes in the River Thames, the United Kingdom[27]. Gleckler et al. (2008) created a set of measurements to accurately measure the relative advantages of CMIP3 models[28]. Aloysius et al. (2016) assessed 25 CMIP5 GCMs in Central Africa regarding historical performance, intermodel and future emission scenario uncertainties[29]. Wang et al. (2019) scored 23 CMIP5 GCMs in an inland basin of Northwest China for the future projections of temperature and precipitation[30]. With the continuous improvement of released CMIP6, several researchers have studied subsets of CMIP6 GCMs, resulting in varied model downscaling. For example, Kreienkamp et al. (2020) downscaled CMIP6 GCM outputs in Germany using the statistical-empirical downscaling approach[31]. Chaudhuri and Robertson (2020) developed the deep neural network model with a structural sensitivity to downscale large-scale annual maximum precipitation from 9 CMIP6 GCMs in Great Bear Lake in Northwest Territories, Canada[32]. However, few studies on SDSM of temperature and precipitation based on CMIP6 outputs have been undertaken.

Hence, in this study, all available CMIP6-GCMs (a total of 17 until November 2021) were assessed by comparing them to observed climatic data, and then downscaled by SDSM across the Ishikari River basin (IRB), which is the most socioeconomically significant basin in Hokkaido, Japan. The primary goals of this study were (1) to select preferred CMIP6 GCMs for the IRB to reduce the uncertainties; (2) to re-establish SDSM predictors between reanalysis datasets of NOAA-CIRES-DOE 20th Century Reanalysis V3 (20CRv3) and CMIP6 GCMs; (3) to project future changes in climatic variables (temperature and precipitation) across the IRB during the mid 21st century (2040–2069, 2040s) and late 21st century (2070–2099, 2070s) under all SSP-RCP scenarios from the CMIP6 GCMs, compared with the baseline period (1985-2014).

Results and Discussions

Selection of GCMs

When assessing GCMs, it is vital to compare GCM outputs with observed records; otherwise, even previous robust predictions may not provide skilled future projections[33]. The observed historical climatic variables were compared to modelled datasets derived from 17 GCMs on the 'historical' experiments from 1985 to 2014, as shown in Figures 1, 2, and 3, which presented by Taylor diagrams of maximum air temperature (tasmax), minimum air temperature (tasmin), as well as precipitation (pr) on the monthly scale at 13 stations. The relative position of GCM points (distance from red dot) on the Taylor diagrams could be used to select appropriate GCMs for each meteorological station. GCMs with high correlations and few errors showed better simulation effects when compared with observed values. For example, at Horokanai, Kamikawa, Furano, and Sapporo stations, in terms of tasmax (Figure 1), GCMs like FGOALS-g3, ACCESS-ESM1-5, MIROC6, and MRI-ESM2-0 (having a correlation coefficient of 0.979, 0.979, 0.978, and 0.982, respectively) were close to observations in Horokanai. MIROC6 and MRI-ESM2-0 performed the highest correlation values in Kamikawa (MIROC6: 0.978, MRI-ESM2-0: 0.981) and Furano (MIROC6: 0.981, MRI-ESM2-0: 0.978). The correlation of FGOALS-g3, ACCESS-ESM1-5, MIROC6 and MRI-ESM2-0 in Sapporo was 0.978, 0.980, 0.980, and 0.980,

respectively, revealing a strong connection between GCMs and observed station data. GCMs such as FIO-ESM-2-0 and MRI-ESM2-0 had the value of RSME lower than 0.25 when assessing *tasmin* in Horokanai and Kamikawa (Figure 2). FGOALS-g3 and MRI-ESM2-0 had the best correlation with tasmin in Furano with a magnitude of 0.976 and 0.975, respectively. The highest correlation magnitudes happened on such GCMs as ACCESS-ESM1-5 (0.983) and MRI-ESM2-0 (0.983) when comparing the tasmin in Sapporo. However, all the GCMs could not well reproduce precipitation (Figure 3). Among 17 GCMs, MIROC6 exhibited the best modeling effects, which was closest to the observations, as shown in Figure 3. The correlations of MIROC6 in Horokanai, Kamikawa, Furano, and Sapporo were only 0.270, 0.370, 0.312, and 0.176, respectively. For each of the climatic variables from 17 CMIP6 GCMs in the study area, similar outputs were obtained from other stations (Figures 1, 2, and 3).

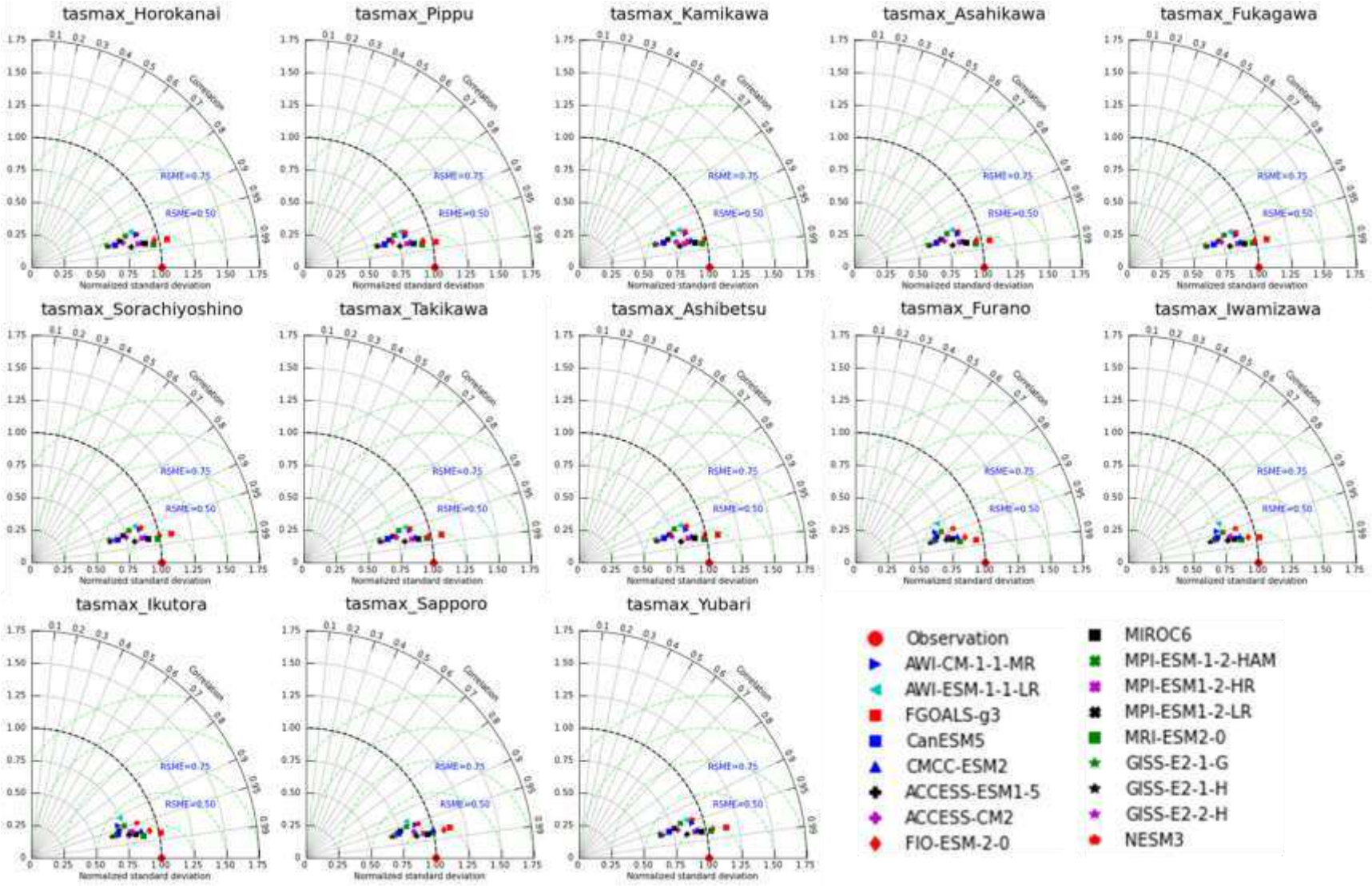

Figure 1 Taylor diagrams of maximum air temperature (tasmax) for each GCM at each station

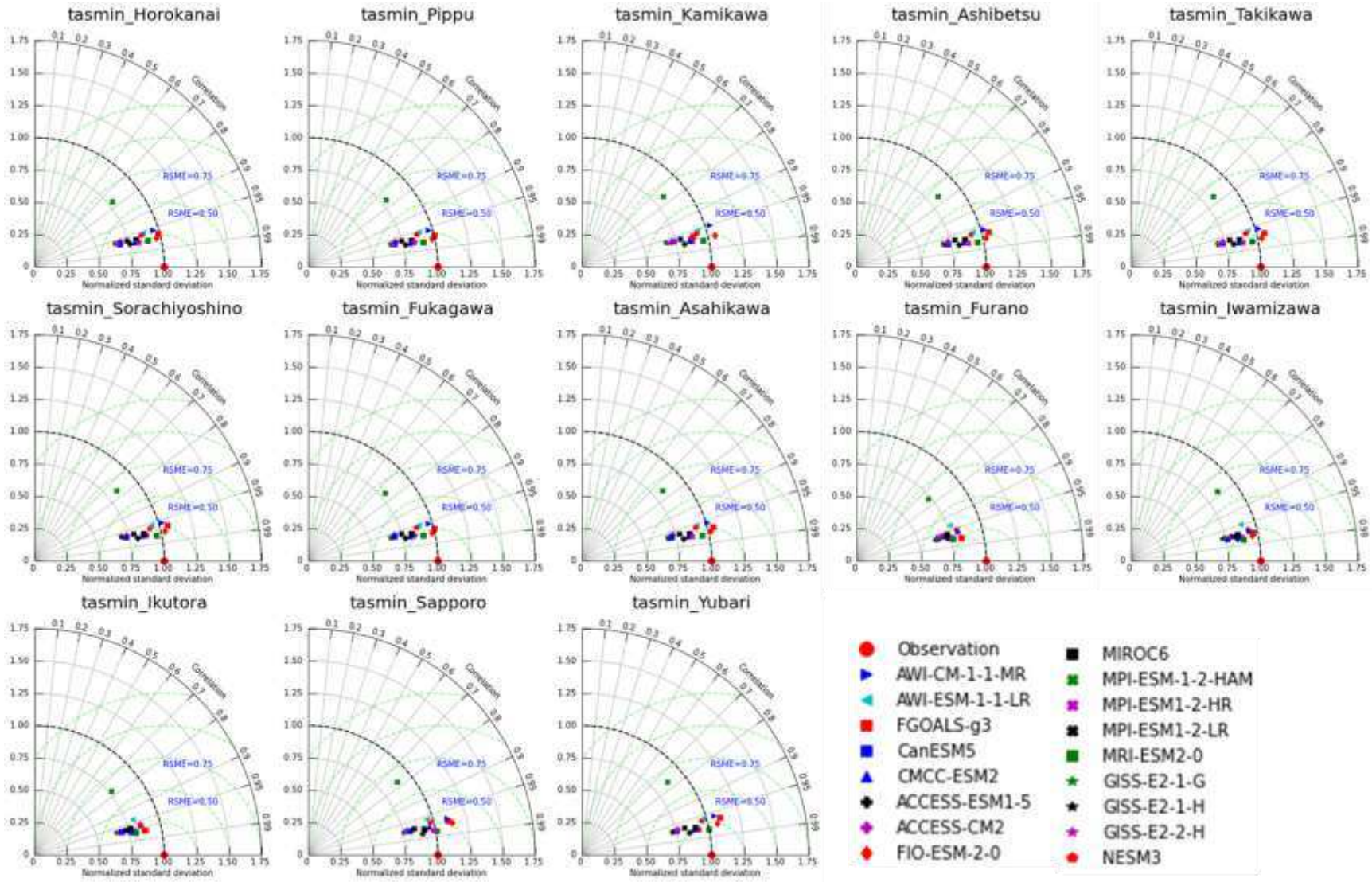

Figure 2 Taylor diagrams of minimum air temperature (tasmin) for each GCM at each station

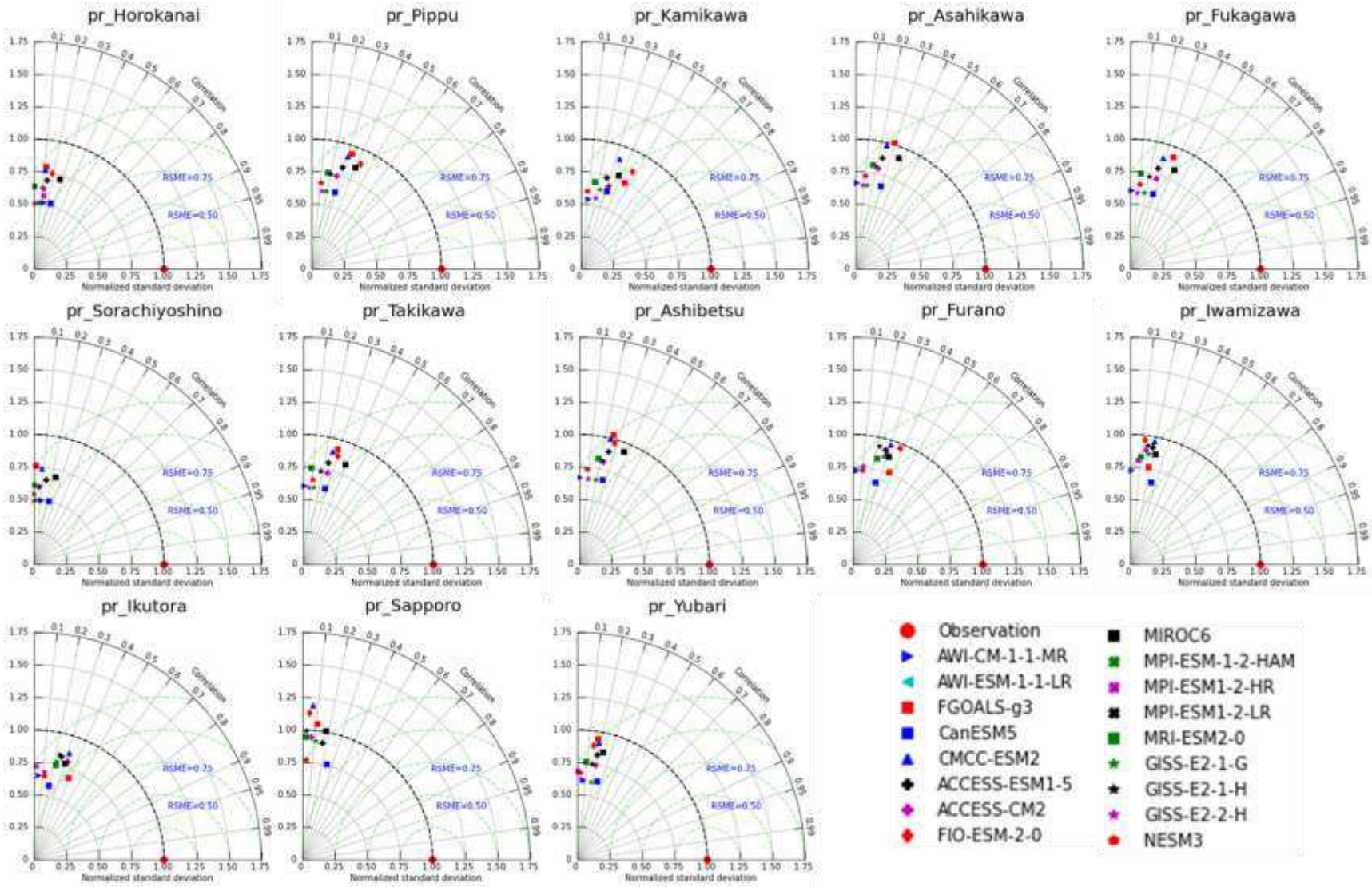

Figure 3 Taylor diagrams of precipitation (pr) for each GCM at each station

SDSM Downscaling

In this study, the span of 1985-1999 was considered as the calibrated phase, and the validated phase was from 2000 to 2014. Table 1 lists the values of four evaluation indexes (like R^2, RMSE, NSE, and Pbais) at 13 meteorological stations when calibrating and validating maximum/minimum air temperature and precipitation on a monthly scale. The R^2 values of each meteorological station's maximum air temperature during the calibrated stage (1985-1999) and validated stage (2000–2014) were 0.954–0.983 and 0.957–0.987, respectively. The R^2 and NSE values of each meteorological station's maximum or minimum air temperatures throughout the simulation phase were nearly equal to 1.000. In terms of maximum air temperature, the values of RSME in these two modeling phases ranged within 0.035-1.065 and 0.089-0.964, respectively. The Pbias values were less than 0.400% in the calibration phase, with the exception of 4.653% at the Horokanai station, and were less than 1.000% in the validation phase, with the exception of 1.374% at the Horokanai station. When simulating the minimum air temperature, RSME values in 1985-1999 and 2000-2014 were 0.034-0.123 and 0.112-0.274, respectively. The absolute values of Pbias were 0.03-9.84% in the downscaling phases. Satisfactory index ranges revealed that SDSM could well simulate maximum/minimum temperatures across the IRB. When accessing the precipitation, the R^2 values of 13 stations ranged from 0.980 to 0.996 during the calibration phase and from 0.957 to 0.986 during the validation phase. The values of RSME spanned from 4.13 to 19.50 in these two modeling phases. The NSE values in both two phases were greater than 0.978. The absolute values of Pbias in these two phases were 2.99-5.02% and 1.79-14.34%, respectively. The Pbias of precipitation at the Yubari station reached 14.34% during the validation phase. The downscaling in SDSM during the calibration phase performed better than that in the validation phase. Meanwhile, the outcomes demonstrated that SDSM outperforms precipitation in modeling tasmax and tasmin. Precipitation is always difficult to simulate due to its high dynamic properties[34]. Generally, choosing an effective mix of predictors for SDSM is challenging owing to influencing variables such as dry and wet period durations, local microclimates, and terrains, which could not be fully covered in reanalysis datasets[35]. In this study, results in downscaling temperature and precipitation demonstrated that predictors from the 20CRv3 dataset are able to reflect attributes on a local scale. In total, SDSM performs effectively in simulating the climatic variables during both calibration and validation phases across the IRB.

255 **Table 1 SDSM-based evaluation index of each station during the phases of calibration (1985-1999) and validation (2000-2014)**

Periods	Predictand	Evaluation index	Meteorological station												
			Horokanai	Pippu	Kamikawa	Asahikawa	Fukagawa	Sorachiyoshino	Takikawa	Ashibetsu	Furano	Iwamizawa	Ikutora	Sapporo	Yubari
Calibration (1985-1999)	Maximum temperature	R^2	0.997	1.000	1.000	1.000	1.000	1.000	1.000	1.000	1.000	1.000	1.000	1.000	1.000
		RMSE	1.065	0.051	0.035	0.044	0.057	0.038	0.045	0.046	0.078	0.081	0.073	0.062	0.036
		Pbias (%)	4.653	0.092	-0.012	-0.056	-0.031	0.084	-0.011	-0.025	0.239	-0.217	-0.352	-0.058	0.054
		NSE	0.988	1.000	1.000	1.000	1.000	1.000	1.000	1.000	1.000	1.000	1.000	1.000	1.000
	Minimum temperature	R^2	1.000	1.000	1.000	1.000	1.000	1.000	1.000	1.000	1.000	1.000	1.000	1.000	1.000
		RMSE	0.088	0.043	0.052	0.075	0.035	0.040	0.058	0.052	0.088	0.123	0.099	0.035	0.034
		Pbias (%)	0.490	0.612	-1.773	0.341	0.312	-0.896	0.284	0.214	-0.948	1.661	9.837	-0.044	-0.036
		NSE	1.000	1.000	1.000	1.000	1.000	1.000	1.000	1.000	1.000	1.000	1.000	1.000	1.000
	Precipitation	R^2	0.991	0.988	0.980	0.987	0.981	0.991	0.994	0.995	0.994	0.987	0.996	0.992	0.989
		RMSE	6.126	5.450	6.444	4.561	5.979	6.849	4.962	4.125	5.212	5.988	5.567	5.710	6.461
		Pbias (%)	-3.259	-3.935	-3.310	-2.994	-3.992	-3.712	-3.810	-3.651	-4.063	-4.531	-4.582	-5.025	-4.331
		NSE	0.997	0.995	0.995	0.997	0.994	0.997	0.997	0.998	0.995	0.995	0.995	0.995	0.996
Validation (2000-2014)	Maximum temperature	R^2	0.998	1.000	1.000	1.000	1.000	1.000	1.000	1.000	1.000	1.000	1.000	1.000	1.000
		RMSE	0.964	0.125	0.097	0.119	0.102	0.098	0.089	0.103	0.142	0.119	0.140	0.111	0.120
		Pbias (%)	1.374	0.197	0.242	0.328	0.151	0.010	0.104	0.165	0.805	0.088	0.988	0.278	0.190
		NSE	0.991	1.000	1.000	1.000	1.000	1.000	1.000	1.000	1.000	1.000	1.000	1.000	1.000
	Minimum temperature	R^2	1.000	1.000	1.000	1.000	0.999	1.000	1.000	1.000	0.999	1.000	1.000	1.000	1.000
		RMSE	0.220	0.209	0.199	0.197	0.238	0.192	0.178	0.205	0.274	0.154	0.222	0.112	0.149
		Pbias (%)	0.923	1.752	0.926	0.432	-0.570	-0.282	0.229	-0.030	2.582	-0.512	-0.130	-0.031	0.497
		NSE	1.000	1.000	1.000	1.000	1.000	1.000	1.000	1.000	1.000	1.000	1.000	1.000	1.000
	Precipitation	R^2	0.962	0.986	0.984	0.970	0.971	0.974	0.957	0.977	0.980	0.974	0.961	0.983	0.972
		RMSE	9.175	5.751	7.318	6.967	7.916	9.489	8.765	6.215	6.659	6.580	9.986	12.768	19.497
		Pbias (%)	-1.794	-3.366	-3.081	-3.087	-2.595	-3.707	-1.887	-2.297	-3.839	-3.431	-4.331	11.441	14.336
		NSE	0.994	0.996	0.994	0.993	0.992	0.995	0.991	0.995	0.993	0.995	0.988	0.984	0.978

256

257

258

Analysis of climatic variables at each station

Observed variables in the historical period (1985-2014) were compared to selected GCMs (MIROC6 and MRI-ESM-2.0). Each GCM has eight SSP-RCPs scenarios, SSP1-1.9, SSP1-2.6, SSP2-4.5, SSP3-7.0, SSP4-3.4, SSP4-6.0, SSP5-3.4OS, and SSP5-8.5. Figures 4, 5, and 6 presented projected annual changes (2015-2100) in mean maximum temperature, minimum temperature, as well as precipitation, respectively, at 13 meteorological stations over the IRB.

As illustrated in Figures 4 and 5, there is a noticeable warming trend in the IRB under all scenarios. SSP5-8.5 may force the most severe warming effect in the future, while SSP1-1.9 may have the least. When compared to the observed tasmax of the reference period, the tasmax was estimated to increase by 1.72-3.47 ℃ in the 2040s and 1.72-3.53 ℃ in the 2070s under SSP1-1.9 of MRIOC6 and rise by 1.97-3.70 ℃ in the 2040s and 1.81-3.53 ℃ in the 2070s under SSP1-1.9 of MRI-ESM-2.0. In the projection of SSP5-8.5 scenario, the tasmax may ascend by 2.94-4.58 °C in the 2040s and 5.50-7.19 °C in the 2070s under MRIOC6, and climb by 3.30-5.12 °C in the 2040s and 4.82-6.74 °C in the 2070s under MRI-ESM-2.0, compared to the reference phase. Meanwhile, the tasmin was predicted to involve fewer variations of warming compared to tasmax at all meteorological stations. The increasing ranges of 2.22-4.87 ℃ in the 2040s and 4.08-6.81 ℃ in the 2070s for tasmin were simulated under SSP5-8.5 of MRIOC6, and 2.60-5.16 ℃ in the 2040s and 3.88-6.48 ℃ in the 2070s under SSP5-8.5 of MRI-ESM-2.0 were simulated. In scenario SSP1-1.9, the tasmin went up by 1.31-3.89 °C in the 2040s and 1.30-3.93 °C in the 2070s under MRIOC6, and increased by 1.53-4.05 °C in the 2040s and 1.35-3.90 °C in the 2070s under MRI-ESM-2.0, as relative to the reference stage. Meanwhile, temperature in the far-future period (2070s) is anticipated to exhibit greater changes than that in the middle period (2040s). The mean temperature was predicted to increase by 2.04-4.52 ℃ under all scenarios during the 2040s, and by 2.67-4.94 ℃ in the 2070s. Annual variations in precipitation showed more discrepancies not only at different meteorological stations but also under different SSP-RCPs scenarios from two GCMs (Figure 6). For example, at the Pippu, Kamikawa, Takikawa, and Ashibetsu stations, SSP-RCPs scenarios from MIROC6 generated higher annual precipitation than those in MRI-ESM-2.0. But at other stations such as Horokanai, Scenario SSP1-1.9 from MRI-ESM-2.0 could predict more precipitation than that in MRIOC6. As shown in Figure 6, annual precipitation was expected to drop at most stations. With the increase of CO_2 emissions, the precipitation presented a tendency opposite to that of temperature. Precipitation will reduce with the temperature rising in the IRB. Particularly, precipitation in the far-future phase was predicted to decrease more than that in the middle period. Under all scenarios of MIROC6, the mean annual precipitation is likely to decrease by 2%-17% during the 2040s, except that the Pippu, Kamikawa, Takikawa, and Ashibetsu stations may have their precipitation increased by 25%, 20%, 17%, and 13%, respectively, while during the 2070s, it may reduce by 7%-20%, except that the Pippu, Kamikawa, Takikawa, and Ashibetsu stations may have their precipitation increased by 19%, 15%, 10%, and 7%, respectively. Under all scenarios of MRI-ESM-2.0, the reduction of rainfall is expected to reach 0.1%-15% in the 2040s and 0.02%-17% in the 2070s.

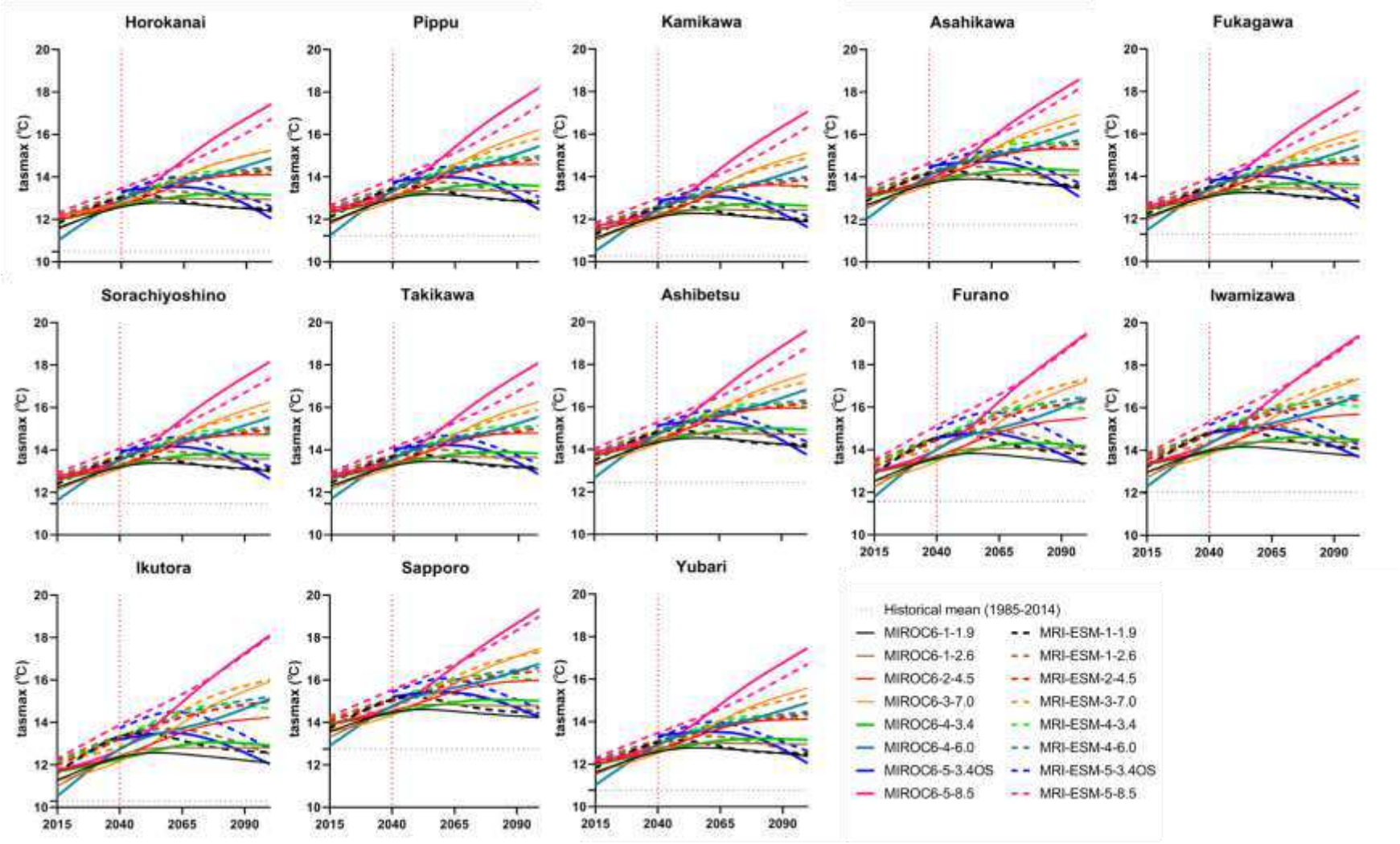

301 **Figure 4 Annual mean maximum temperature (tasmax) under SSP-RCPs scenarios of two GCMs**

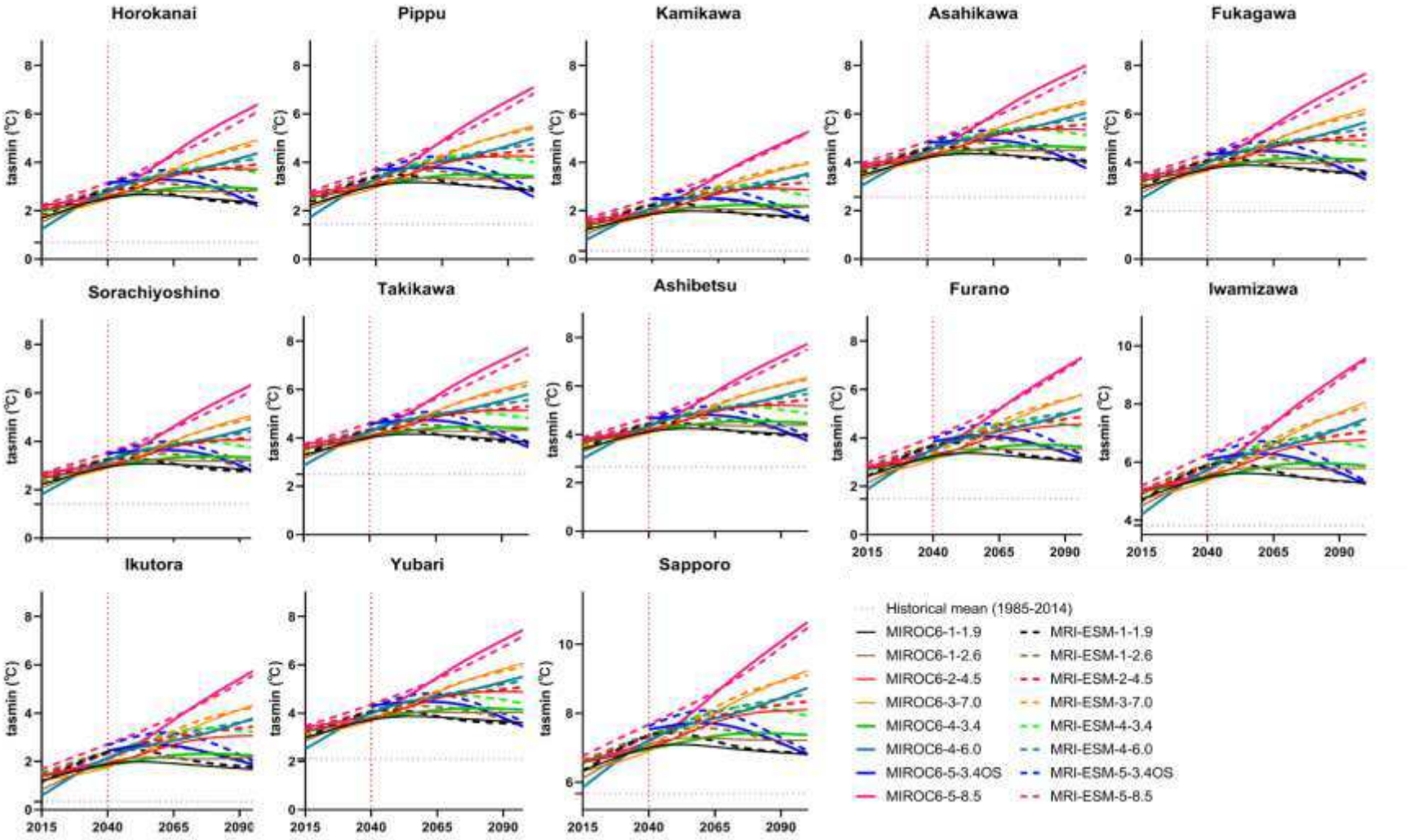

Figure 5 Annual mean minimum temperature (tasmin) under SSP-RCPs scenarios of two GCMs

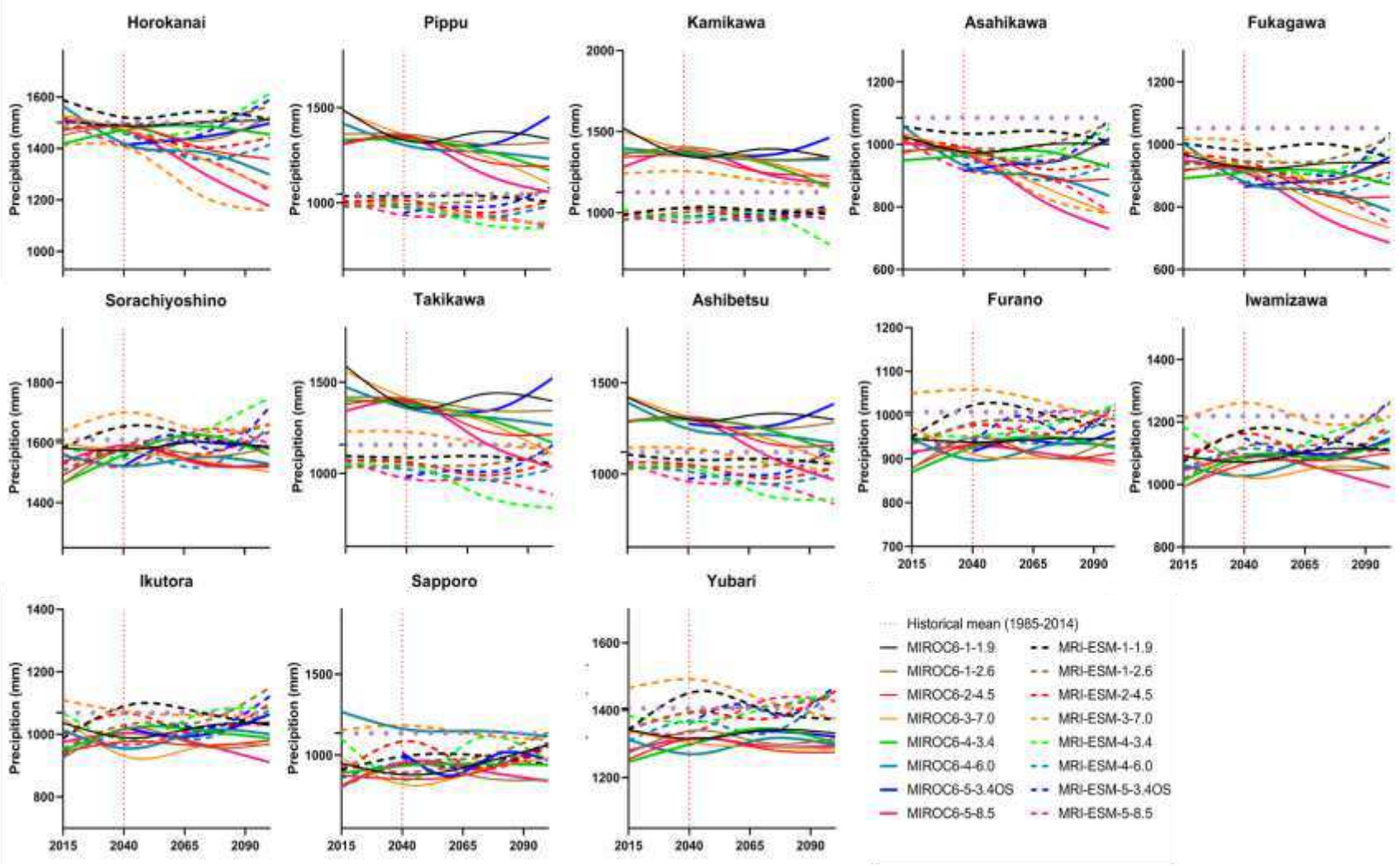

Figure 6 Annual mean precipitation under SSP-RCPs scenarios of two GCMs

Projection of climatic variables

Figures 7 and 8 showed the variations in average climatic variables (tasmax, tasmin, and precipitation) of all meteorological stations under MIROC6 and MRI-ESM-2.0 scenarios in two phases of 2040s and 2070s, in respect to the reference stage of 1985-2014. The SSP-RCP scenarios had a clear impact on temperature and rainfall. Scenario SSP5-8.5 always generated the highest temperature in the 2040s and 2070s, with the tasmax and tasmin increasing by 39% and 102% in the 2040s and 39% and 133% in the 2070s , respectively, compared to baseline. Following the SSP5-8.5, SSP3-7.0, SSP4-6.0, SSP4-3.4, SSP2-4.5, SSP5-3.4OS, and SSP1-2.6 scenarios were also likely to increase temperature. The scenario SSP1-1.9 projected the least increase in tasmax (2040s: 17%, 2070s: 18%) and tasmin (2040s: 70%, 2070s: 105%). The emission scenario had a greater impact on temperature and precipitation projection than the socioeconomic scenario. The increasing range is from the high-emission (SSP5-8.5) to the low-emission case (SSP1-1.9). However, precipitation exhibited opposite variations under SSP-RCP scenarios compared to tasmax and tasmin. SSP1-1.9 always produced the greatest amount of rainfall, with the percent changes of -2% in the 2040s and 3% in the 2070s, and SSP5-8.5 made the least, with the percent changes of -11% during the 2040s and -2% during the 2070s. Meanwhile, MIROC6 could support a wider range of variations in maximum and minimum temperatures than MRI-ESM-2.0. The percent changes under MIROC6 were 16%-51% for tasmax and 70%-212% for tasmin, respectively. In terms of MRI-ESM-2.0, variations were from 17% to 46% for tasmax and from 79% to 200% for tasmin, respectively. The precipitation changes were -11%- **-**1% under MIROC6 and -11%- 1% under MRI-ESM-2.0.

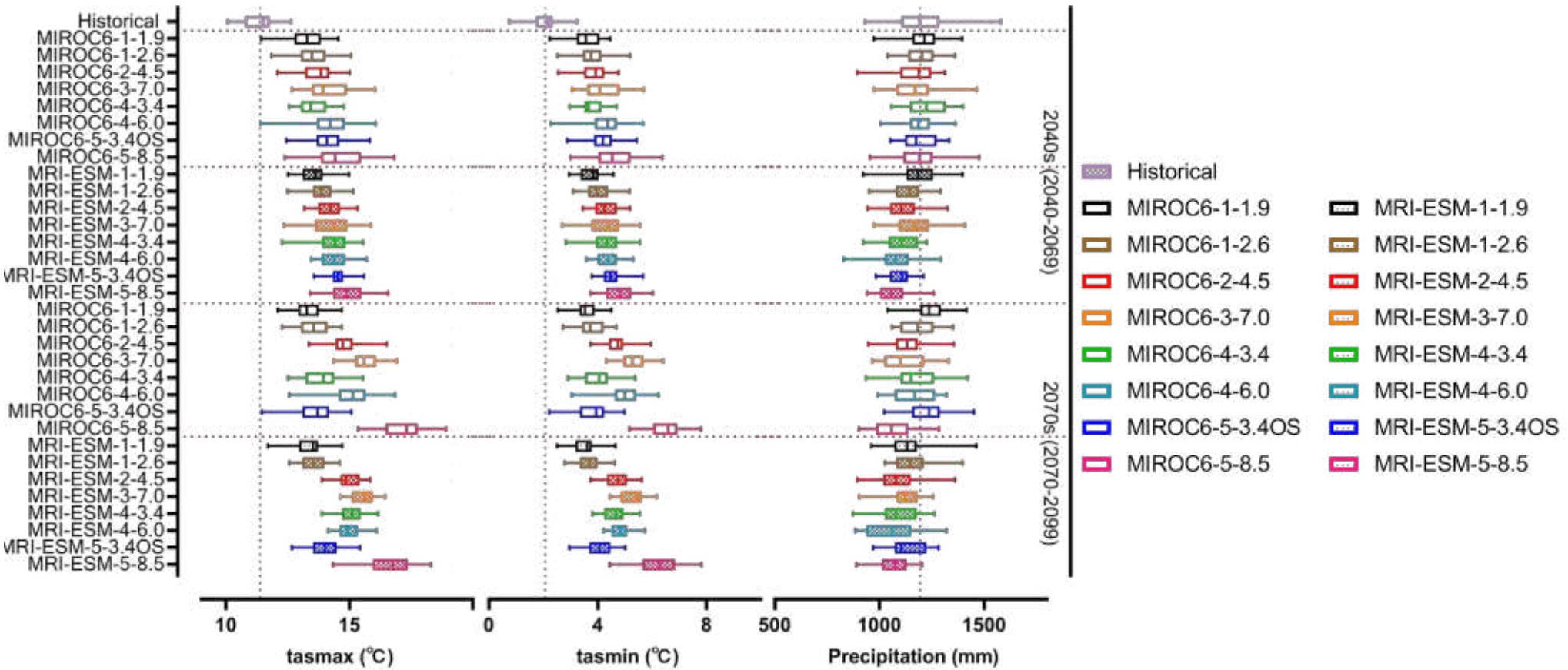

Figure 7 Variations in maximum temperature (tasmax), minimum temperature (tasmin), and precipitation in periods of the 2040s and 2070s under SSP-RCPs scenarios of MIROC6 and MRI-ESM-2.0

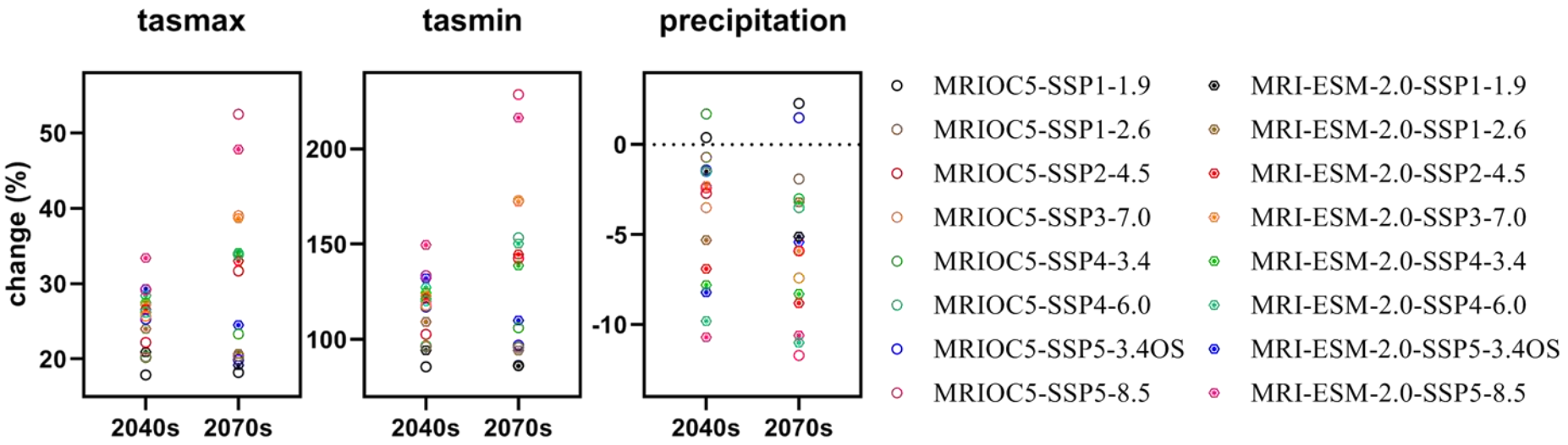

Figure 8 Percent change of average maximum temperature (tasmax), minimum temperature (tasmin), and precipitation in the 2040s and 2070s, with respect to the baseline (1985-2014)

Discussion

In this study, we compared climatic variables (maximum/minimum temperature and precipitation) from all available CMIP6 GCMs at 13 meteorological stations around the IRB. The performances of 17 GCMs were evaluated by Taylor diagrams with correlation coefficient and root-mean-square difference. Most CMIP6 GCMs were able to access temperature measurements with high correlations. But no single GCMs could well reproduce precipitation across the IRB. Two preferred GCMs, MIROC6 and MRI-ESM-2.0 showed the best adaptability in temperature and precipitation across the target region.

Accordingly, in order to generate daily maximum/minimum temperature and daily precipitation in two future phases, the 2040s (2040-2069) and 2070s (2070-2099), a statistical downscaling model was established based on 20CRv3 reanalysis datasets and GCMs-derived predictors, with respect to observed climate during 1985-2014. Constructed SDSM had satisfactory modeling performance in both temperature and precipitation during calibrating (1985-1999) and validating (2000-2014) stages. The values of R^2 and NSE of temperature simulation at each station nearly reached 1.000. The values of R^2 and NSE in terms of precipitation were greater than 0.957. SDSM presented a better ability in simulating temperature than precipitation. CMIP6 GCMs, while showing a significant correlation with temperature measurements, were unable to represent rainfall features in the IRB. Detecting precipitation features derived from climate model simulations is more strenuous relative to temperature[36]. No CMIP3 model could recreate the magnitude of the seasonal precipitation cycle in the western USA[37]. All eleven GCMs from CMIP3 have trouble simulating precipitation in peninsular India[38]. Benedict et al. (2019) also found that CMIP5 GCMs could not improve the precipitation budget of the Mississippi basins[13]. That was because GCMs are incapable of modeling precipitation with high accuracy, e.g., on the local station scale, and the GCM outputs of precipitation are affected by topographical factors and regional climatic forcing[22]. On the other hand, the downscaling process of precipitation further propagates this error[39]. It should be more cautious when downscaling precipitation with SDSM[40]. To sum up, FGOALS-g3, CanESM5, MIROC6, and MRI-ESM2-0 have the best predictive ability of maximum temperature, MRI-ESM2-0 has the best predictive ability of minimum temperature, and MIROC6 has the best predictive ability of precipitation. Given the availability of each GCM with adequate predictors for SDSM simulating, MIROC6 and MRI-ESM2-0 from CMIP6 were chosen to generate future climatic variables under various SSP-RCPs scenarios.

The distribution of average changes in maximum temperature, minimum temperature, as well as precipitation of the IRB during the 2040s and 2070s under the MIROC6 and MRI-ESM-2.0 are displayed in Figures 9, 10, and 11, respectively. MIROC6 and MRI-ESM-2.0 both show high air temperature and low precipitation (Figures 9, 10, and 11). When it came to the distribution of tasmax and tasmin, both products showed a similar trend, with a bigger rise in the northern part and a smaller rise in the southern part of the IRB. According to meteorological data, the northern part was colder than the southern part of the study area, but CMIP6 GCMs anticipated that the northern part may exhibit a stronger warming trend in the future. The precipitation across the IRB showed a decreasing trend under MRI-ESM-2.0. However, a large increase in precipitation produced by MRIOC6 was found in

399 the mid-northern part of the IRB, which was displayed as an absolute difference from MRI-
400 ESM-2.0. Higher temperature and lower precipitation were projected during the late 21st
401 century (2070s) than the mid-century (2040s) in the IRB. The distribution of climatic
402 variable changes was strongly affected by emissions. Higher emissions are associated with
403 higher temperatures and less precipitation under all of the climatic scenarios in this study.

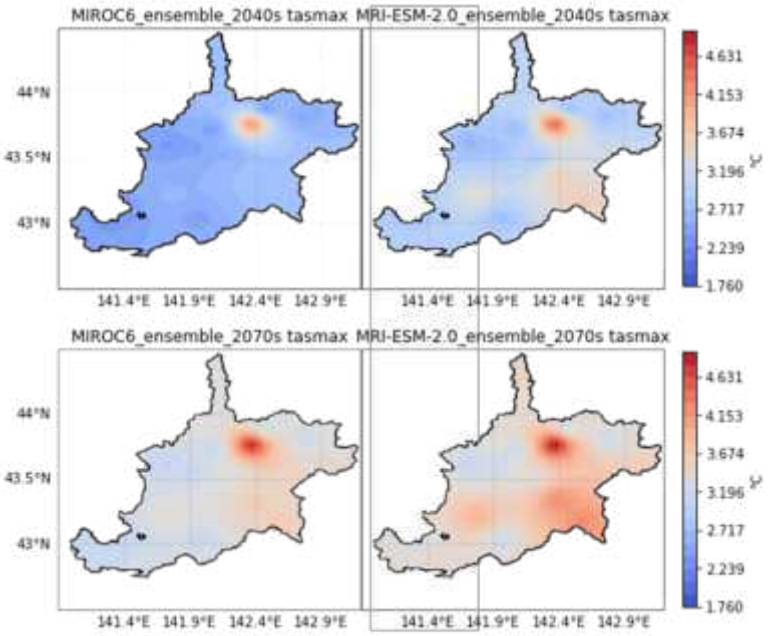

404

405 **Figure 9 Changes in the maximum temperature (tasmax) of the Ishikari River basin in**
406 **periods of the 2040s and 2070s under MIROC6 and MRI-ESM-2.0**

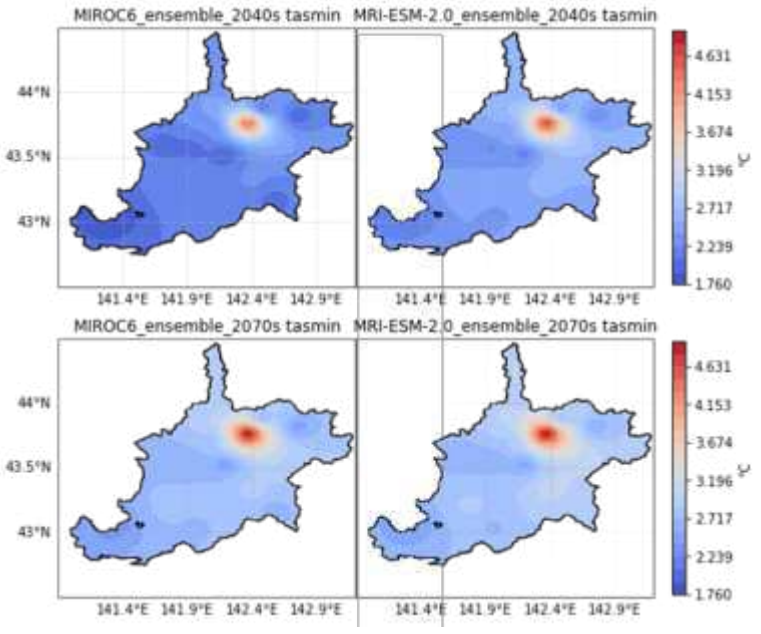

407

408 **Figure 10 Changes in the minimum temperature (tasmin) of the Ishikari River basin in**
409 **periods of the 2040s and 2070s under MIROC6 and MRI-ESM-2.0**

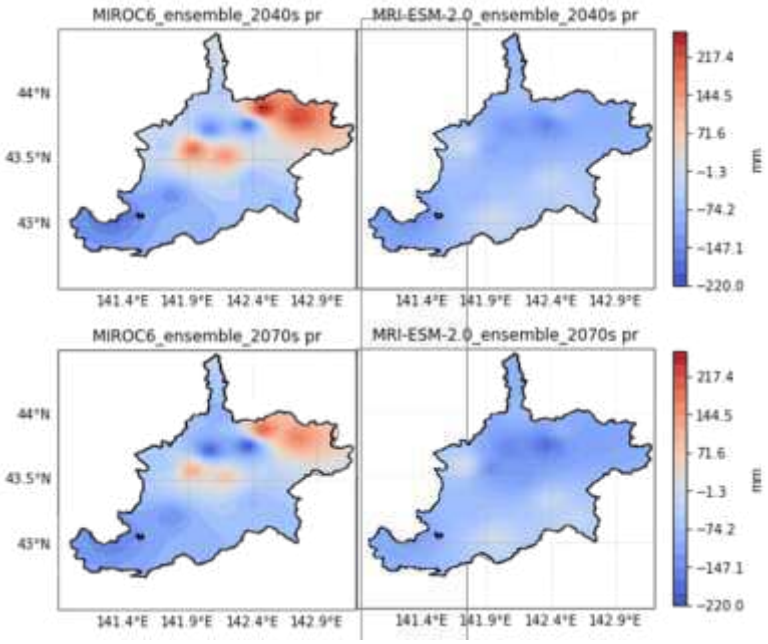

Figure 11 Changes in the annual precipitation (pr) of the Ishikari River basin in periods of the 2040s and 2070s under MIROC6 and MRI-ESM-2.0

Future climatic variables were projected in all SSP-RCP scenarios (SSP1-1.9, SSP1-2.6, SSP2-4.5, SSP3-7.0, SSP4-3.4, SSP4-6.0, SSP5-3.4OS, and SSP5-8.5). Average tasmax and tasmin under eight SSP-RCP scenarios were projected to rise about 2.32-4.84 °C and 1.76-4.91 °C from MIROC6, 2.65-4.93 °C and 2.07-4.95 °C from MRI-ESM-2.0, respectively. MIROC6 and MRI-ESM-2.0 generated future rainfall with a decreased trend by -6% and -5%, respectively. Temperature changes in the far-future period (2070s) may be larger than those in the middle period (2040s). The average temperature was anticipated to rise by 2.04-4.52 °C under all scenarios during the 2040s, and by 2.67-4.94 °C during the 2070s. SSP-RCP scenarios could provide a wider variation range of climatic variables to eliminate further uncertainties when projecting future climate change scenarios. Outputs forecast plausible future climate change in the IRB. The datasets of climatic variables established in this work can be utilized in regional or local hydrologic and environmental modeling, as well as analyzing the sustainability of ecosystems.

Materials and Methods

Study area

The Ishikari River basin (IRB (42°41′9.6″N-44°47′8.9″N, 140°59′33″E-143°10′47.8″E) was situated in the Mid-western Hokkaido, Japan, with an area of 14,330 km^2 (Figure 12). The Ishikari River originates from Mt. Ishikari and flows westward to the Sea of Japan. Toyohira, Tobetsu, Chitose, and Yubari are its major tributaries[41]. 52% of the population of Hokkaido live in the IRB. The IRB is an important economic, agricultural, industrial, and cultural center of Hokkaido, and is also the seat of Sapporo and Asahikawa, the largest two cities of Hokkaido. The IRB is dominantly controlled by the hot-summer subtype and hemiboreal climate. According to the climate records (1985-2014) of 13 meteorological stations across the IRB provided by the Japan Meteorological Agency (JMA,

http://www.jma.go.jp), the annual average maximum and minimum temperatures are 10.27-12.74 ℃ and 0.34-5.67 ℃, respectively. The annual precipitation is about 1,007-1,610 mm. The rainy season is generally from August to September. The snowfall period is from mid-December to late March of the following year, with an average annual maximum snow depth of 35 cm. Hydrologic peaks occur during the snow-melt period (March to May).

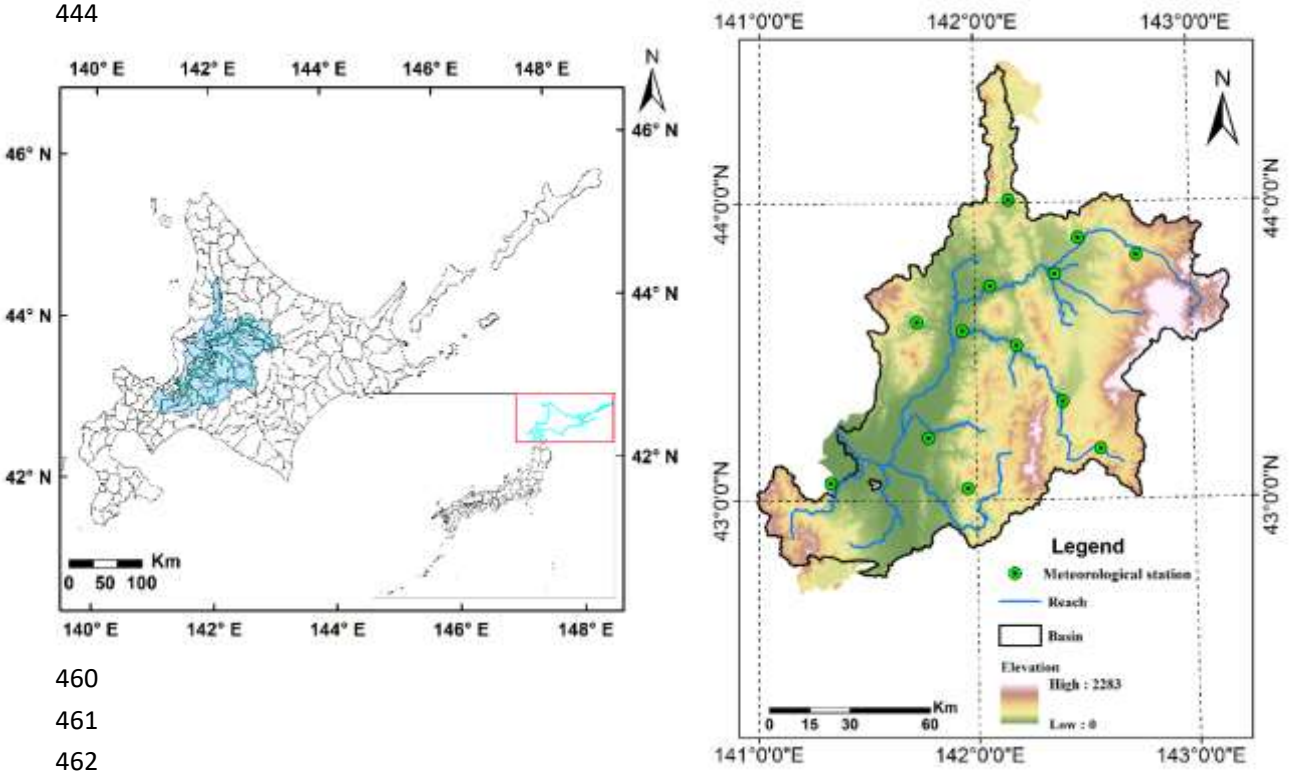

Figure 12 Locations of the Ishikari River basin (IRB) and its meteorological stations

Data collection

Three types of meteorological datasets were employed in this study, including observed historical data, reanalysis data, and GCM data. IRB covered 13 meteorological stations (as shown in Figure 12). The historical meteorological data across 30 years period of 1985-2014 was composed of daily maximum air temperature at 2 m (tasmax), daily minimum air temperature at 2 m (tasmin), and daily precipitation (pr) of each meteorological station, which can be accessed in the JMA.

In this study, the reanalysis dataset selected the most recent version of reanalysis from the Twentieth Century Reanalysis (20CR) Project, which is funded by the National Oceanic and Atmospheric Administration (NOAA), the Cooperative Institute for Research in Environmental Sciences (CIRES), and the U.S. Department of Energy (DOE), NOAA-CIRES-DOE 20th Century Reanalysis V3 (20CRv3). The 20CRv3 contained objectively-analyzed 4-dimensional weather maps and their uncertainties[42]. The 20CRv3 covered the spatial resolution of 1.0-degree latitude x 1.0-degree longitude global grid (360x181). Daily atmospheric variables (such as humidity, precipitation flux, and geopotential height) of 20CRv3, spanning 1985 to 2014, were readily accessible at the NOAA Physical Sciences

Laboratory (PSL, https://www.psl.noaa.gov/).

Monthly and daily GCM datasets under the first variant level "r1i1p1f1" were obtained from the Coupled Model Intercomparison Project Phase 6 (CMIP6, https://esgf-node.llnl.gov/search/cmip6/). According to the availability of predictors, 17 GCMs were selected in this study, as shown in Table 2. All these predictors were interpolated onto a 1° × 1° grid to match the 20CRv3. The GCMs-derived monthly variables (tasmax, tasmin and pr) in the period of 1985-2014 were applied for the selection of GCMs.

The daily atmospheric predictors (corresponding to 20CRv3), spanning 1985-2100, were applied in statistical downscaling analysis to generate and project future climatic variables under eight Shared Socioeconomic Pathways-Representative Concentration Pathways (SSP-RCPs) scenarios (SSP1-1.9, SSP1-2.6, SSP4-3.4, SSP2-4.5, SSP4-6.0, SSP3-7.0, SSP5-3.4OS, and SSP5-8.5). CMIP6 used a matrix framework that combined two determinants of emission scenarios (like RCPs) and different socioeconomic assumptions, namely the so-called Shared Socioeconomic Pathways (SSPs) scenarios, to force climate models[16,43,44], which makes future scenarios more reasonable.

The growth of civilization and natural systems at the national and regional levels in the twenty-first century provides a foundation for the formation of SSPs[45]. Five narratives of SSP (SSP1, SSP2, SSP3, SSP4, and SSP5) scenarios were employed to picture the potential challenges brought about by the variations in global and regional evolution across time[46,47]. Numbers are consistent with low-to-high concerns in mitigation and adaptation in the futuristic society, named SSP1 ("taking the green road"), SSP2 ("a middle of the road"), SSP3 ("regional rivalry – a rocky road"), SSP4 ("inequality – a road divided"), and SSP5 ("fossil-fueled development"), respectively[48]. Among those SSP-RCPs scenarios, SSP1-2.6, SSP2-4.5, SSP4-6.0, and SSP5-8.5 are upgraded versions of RCP2.6, RCP4.5, RCP6.0, and RCP8.5 in CMIP5, respectively. The novel scenario includes SSP1-1.9, SSP4-3.4, SSP3-7.0, and SSP5-3.4OS[49]. SSP1-1.9 assumes keeping the temperature increase below 1.5℃ over pre-industrial levels by 2100. SSP4-3.4 attempts to investigate the gap between scenarios RCP2.6/SSP1-2.6 (< 2 ℃) and RCP4.5/SSP2-4.5 (approximately 3℃) at the end of 21st century. SSP5-3.4OS is an overrun scenario (OS) wherein emissions maintain a much worse SSP5-8.5 trajectory until 2040, but after they plummet abruptly, late-century negative emissions may increase. New scenarios might provide scientists with a broader range of scenarios to model impacts on climate change[50].

514 **Table 2 Available CMIP6 GCMs sources and information**

No.	GCMs	Institution	Nominal Resolution (km)
1	AWI-CM-1-1-MR	Alfred Wegener Institute, Helmholtz Centre for Polar and Marine Research, Germany	100
2	AWI-ESM-1-1-LR		250
3	FGOALS-g3	Chinese Academy of Sciences, China	250
4	CanESM5	Canadian Centre for Climate Modelling and Analysis, Environment and Climate Change Canada, Canada	500
5	CMCC-ESM2	Fondazione Centro Euro-Mediterraneo sui Cambiamenti Climatici, Italy	100
6	ACCESS-ESM1-5	Commonwealth Scientific and Industrial Research Organisation, Australia	250
7	ACCESS-CM2	Commonwealth Scientific and Industrial Research Organisation, Australia & ARCCSS (Australian Research Council Centre of Excellence for Climate System Science)	250
8	FIO-ESM-2-0	FIO (First Institute of Oceanography, Ministry of Natural Resources, China) & QNLM (Qingdao National Laboratory for Marine Science and Technology, China)	100
9	MIROC6	JAMSTEC (Japan Agency for Marine-Earth Science and Technology, Japan) & AORI (Atmosphere and Ocean Research Institute, The University of Tokyo, Japan) & NIES (National Institute for Environmental Studies, Japan) & R-CCS (RIKEN Center for Computational Science, Japan)	250
10	MPI-ESM-1-2-HAM	Max Planck Institute for Meteorology, Germany	250
11	MPI-ESM1-2-HR		100
12	MPI-ESM1-2-LR		250
13	MRI-ESM2-0	Meteorological Research Institute, Japan	100
14	GISS-E2-1-G	Goddard Institute for Space Studies, USA	250
15	GISS-E2-1-H		250
16	GISS-E2-2-H		250
17	NESM3	Nanjing University of Information Science and Technology, China	250

515

Evaluation of GCMs performance

GCMs are extensively applied to simulate past climates and produce future climatic variables[51]. However, there is a significant uncertainty in estimating regional applications of GCMs due to the difference in each GCM, such as resolution (fine or coarse), climatic response mechanism (aerosols, circulations of land, ocean, and atmosphere), and spatial-temporal scales[52]. Hence, there is an urgent need to analyze each chosen GCM to minimize the uncertainties when applying them in specific areas. Evaluating the performance of GCMs simulation is generally to compare them with reanalysis or observed climatic data. Lots of indicators have been employed by various researchers in climate modelling. Raju and Kumar (2020) reviewed more than hundreds of works on climate models to study which are the best GCMs[53]. They recommended using category-wise indicators when evaluating GCMs, such as error and correlation coefficient. The Taylor diagram can compare simulations (model) with measurements using the correlation coefficient, root-mean-square difference, and standard deviations to graphically assess these qualities[54]. The high correlation and few errors represent that selected GCMs are suitable for the local climate system. Therefore, the Taylor diagram was used in this work to compare CMIP6 outputs with regional data and further to identify the best CMIP6 GCMs for modeling temperature and precipitation across the IRB.

The Statistical DownScaling Model

Description

SDSM, designed by Wilby et al. (2002), is a decision-making support tool for analyzing the implications of local climate changes[21]. SDSM 4.2, based on the Visual Basic programme, was widely used in many climate-related investigations[22]. SDSM can set up statistical relationships between large-scale predictors and regional-scale climatic conditions (e.g., temperature and precipitation) using a combination of multiple linear regressions. If these correlations remain true as in prospective, they may be utilized to acquire downconverted regional features in certain coming phases by forcing the interactions with GCM-derived predictors through the stochastic weather generator. There are two different progress in each sub-model, unconditional and conditional. Temperature does not need to be transformed and directly generated in the unconditional pattern, which exhibits a linear relationship between the predictors and predictand (e.g., individual wind speeds can be used to calculate regional airflow parameters). Precipitation should be reformed by the fourth root and then simulated in the conditional pattern, which is an intermediate process between regional forcing and local climatic conditions. For instance, local precipitation is determined by the occurrence of rainy days, while the latter is determined by regional-scale predictors (such as moisture and atmospheric pressure). The wet criterion for daily rainfall was chosen at 1.0 mm in this study, as it is commonly employed for statistical downscaling.

Model process

SDSM performs five key steps, from variables selection, calibrating and validating model, to weather generation and future climate scenarios projection[55]. Screening variables

between predictand (such as maximum temperature, minimum temperature, evaporation, as well as precipitation on a local scale) and predictor (large-scale atmospheric conditions) is a core of the statistical downscaling process. SDSM combines the correlation matrix, partial correlation, P value, histograms, and scatter plots, which can help users to find the best predictors. Peng et al. (2021) provided extensive explanations of each SDSM procedure[56].

In this study, predictors were constructed by the reanalysis datasets (20CRv3) and CMIP6 GCMs to reproduce ensembles of present climate data in SDSM. Commonly used predictors are normalized and obtained as predictor datasets. In this study, predictors are comprised of mean temperature at 2 m (temp), mean sea level pressure (mslp), total precipitation (prcp), surface downwelling longwave flux in air (rlds) and surface downwelling shortwave flux in air (rsds) in monolevel, specific humidity (#_shum), relative humidity (#_rhum), geopotential height (_p), geostrophic air flow velocity (#_f), vorticity (#_z), zonal velocity component (#_u), meridional velocity component (#_v), divergence (#_zh), and wind direction (#_th) under the pressure level (# refers to heights of 500 hPa, 700 hPa, 850 hPa, as well as 1,000 hPa). Table 3 lists the most suitable predictors for observed predictands in 13 meteorological stations across the IRB. Simulation of precipitation needs more predictors other than temperature.

Table 3 List of selected predictors in the Ishikari River basin

Stations	Predictand		
	tasmax	tasmin	pr
Horokanai	1000shum, temp, 500p	1000shum, temp, rlds	1000u, rsds, 700p, 850rhum
Pippu	1000shum, temp, 500p	1000shum, temp, rlds	1000u, rsds, 700p, 800p, 850rhum, 1000rhum
Kamikawa	1000shum, temp, 500p	1000shum, temp	rsds, 700p, 800p, 850rhum
Asahikawa	1000shum, temp, 500p	1000shum, temp, rlds	1000u, rsds, 700p, 850rhum
Fukagawa	1000shum, temp, 500p	1000shum, temp, rlds	1000u, rsds, 700p,850rhum,
Sorachiyoshino	1000shum, temp, 500p	1000shum, temp, rlds	1000u, rsds, 700p, 800p, 850rhum
Takikawa	1000shum, temp, 500p	1000shum, temp	1000u, rsds, 700p, 850rhum
Ashibetsu	1000shum, temp, 500p	1000shum, temp	rsds, 700p, 850rhum
Furano	1000shum, temp, 500p	1000shum, temp	rsds, 700p, 850p, 850rhum
Iwamizawa	1000shum, temp, 500p	1000shum, temp	1000u,700p, 850p, 850rhum, prcp
Ikutora	1000shum, temp, 500p	1000shum, temp	1000u, rsds, 700p, 850p, 850rhum, prcp
Sapporo	1000shum, temp, 500p	1000shum, temp	700p,850p, 7000rhum, 850rhum, prcp
Yubari	1000shum, temp, 500p	1000shum, temp	rsds, 700p,850p, 850rhum

SDSM evaluation

Generally speaking, the model's performance is mainly based on the selection step for predictors to predictands in SDSM. Even though there are statistical or graphical ways, such as correlation matrix and P value during the screening process, to identify the most accurate predictors, applying statistical parameters in the evaluation process is necessary to avoid uncertainties in SDSM. The ability of modeling outputs from SDSM was obtained by determining the Nash and Sutcliffe efficiency (NSE, Eq. 1), coefficient of determination (R^2, Eq. 2), root mean square error (RMSE, Eq. 3), and percent bias ($P_{bias,}$ Eq. 4).

The magnitude of NSE is computed using the formula below:

585 $$NSE = 1 - \frac{\sum_{i=1}^{n}(X_{oi}-X_{mi})^2}{\sum_{i=1}^{n}(X_{oi}-\overline{X}_{mi})^2} \quad \text{(Eq. 1)}$$

586 The magnitude of R^2 is calculated using the following equation:

587 $$R^2 = \frac{\sum_{i=1}^{n}(X_{oi}-\overline{X}_{oi})(X_{mi}-\overline{X}_{mi})}{[\sum_{i=1}^{n}(X_{oi}-\overline{X}_{oi})^2]^{0.5}[\sum_{i=1}^{n}(X_{mi}-\overline{X}_{mi})^2]^{0.5}} \quad \text{(Eq. 2)}$$

588 The magnitude of RMSE is computed using the formula below:

589 $$RMSE = \sqrt{\frac{\sum_{i=1}^{N}(X_{oi}-X_{mi})^2}{N}} \quad \text{(Eq. 3)}$$

590 The magnitude of Pbias is calculated using the following equation:

591 $$P_{bias} = \frac{\sum_{i=1}^{N}(X_{mi}-X_{oi})}{\sqrt{\sum_{i=1}^{N}X_{oi}}} \times 100 \quad \text{(Eq. 4)}$$

592 where X_{oi} is the observed predictand on day i, X_{mi} is the modeling outcome on day
593 i, $\overline{X}_{oi}$ is the average measured value during the study period, and n is the total number
594 of the observed data. The NSE illustrates how well the observed and simulated data suit
595 the 1:1 line. Both R^2 and *RMSE* are indices of quality of fit, whereas *Pbias* reveals the
596 model's tendency to over- or under-estimated with respect to the observed data. The
597 model performs well when R^2 and NSE values are close to one, and the lower the RMSE
598 and absolute value of Pbias are, the tighter the modeled and measured magnitudes are[57].
599

600 **Acknowledgments**

601 This study is funded by JSPS Grants-in-aid for Scientific Research (No. 26511001).

602 **Data availability**

603 All meteorological datasets during the current study are provided by the Japan
604 Meteorological Agency (JMA, http://www.jma.go.jp). The 20CRv3 datasets are available at
605 the NOAA Physical Sciences Laboratory (PSL, https://www.psl.noaa.gov/). The daily
606 atmospheric predictors are accessed from the Coupled Model Intercomparison Project
607 Phase 6 (CMIP6, https://esgf-node.llnl.gov/search/cmip6/).
608
609

References

1 Osman, M. B. *et al.* Globally resolved surface temperatures since the Last Glacial Maximum. (2021).

2 Mora, C. *et al.* Broad threat to humanity from cumulative climate hazards intensified by greenhouse gas emissions. *Nature Climate Change* 8, 1062-1071 (2018).

3 Calel, R., Chapman, S. C., Stainforth, D. A. & Watkins, N. W. Temperature variability implies greater economic damages from climate change. *Nature communications* 11, 1-5 (2020).

4 Cheng, H. *et al.* Climate change patterns in Amazonia and biodiversity. *Nature communications* 4, 1-6 (2013).

5 Hoegh-Guldberg, O. *et al.* The human imperative of stabilizing global climate change at 1.5 C. *Science* 365 (2019).

6 Smith, C. J. *et al.* Current fossil fuel infrastructure does not yet commit us to 1.5 C warming. *Nature communications* 10, 1-10 (2019).

7 Wheater, H. S. Flood hazard and management: a UK perspective. *Philosophical Transactions of the Royal Society A: Mathematical, Physical and Engineering Sciences* 364, 2135-2145 (2006).

8 Themeßl, M. J., Gobiet, A. & Heinrich, G. Empirical-statistical downscaling and error correction of regional climate models and its impact on the climate change signal. *Climatic Change* 112, 449-468 (2012).

9 Meehl, G. A. *et al.* The WCRP CMIP3 multimodel dataset: A new era in climate change research. *Bulletin of the American meteorological society* 88, 1383-1394 (2007).

10 Taylor, K. E., Stouffer, R. J. & Meehl, G. A. An overview of CMIP5 and the experiment design. *Bulletin of the American meteorological Society* 93, 485-498 (2012).

11 Orlowsky, B. & Seneviratne, S. I. Global changes in extreme events: regional and seasonal dimension. *Climatic Change* 110, 669-696 (2012).

12 Su, B. *et al.* Insight from CMIP6 SSP-RCP scenarios for future drought characteristics in China. *Atmospheric Research* 250, 105375 (2021).

13 Benedict, I., Heerwaarden, C. C. v., Weerts, A. H. & Hazeleger, W. The benefits of spatial resolution increase in global simulations of the hydrological cycle evaluated for the Rhine and Mississippi basins. *Hydrology and Earth System Sciences* 23, 1779-1800 (2019).

14 Moss, R. H. *et al.* The next generation of scenarios for climate change research and assessment. *Nature* 463, 747-756 (2010).

15 Xuan, W. *et al.* Evaluating historical simulations of CMIP5 GCMs for key climatic variables in Zhejiang Province, China. *Theoretical and Applied Climatology* 128, 207-222 (2017).

16 Eyring, V. *et al.* Overview of the Coupled Model Intercomparison Project Phase 6 (CMIP6) experimental design and organization. *Geoscientific Model Development* 9, 1937-1958 (2016).

17 O'Neill, B. C. *et al.* Achievements and needs for the climate change scenario framework. *Nature climate change* 10, 1074-1084 (2020).

18 Tang, J. *et al.* Statistical downscaling and dynamical downscaling of regional climate in China: Present climate evaluations and future climate projections. *Journal of Geophysical Research: Atmospheres* 121, 2110-2129 (2016).

19 Schoof, J. T. Statistical downscaling in climatology. *Geography Compass* 7, 249-265 (2013).

20 Wood, A. W., Leung, L. R., Sridhar, V. & Lettenmaier, D. Hydrologic implications of dynamical and statistical approaches to downscaling climate model outputs. *Climatic change* 62, 189-216 (2004).

21 Wilby, R. L., Dawson, C. W. & Barrow, E. M. SDSM—a decision support tool for the assessment of regional climate change impacts. *Environmental Modelling & Software* 17, 145-157 (2002).

22 Wilby, R. L. & Dawson, C. W. The statistical downscaling model: insights from one decade of application. *International Journal of Climatology* 33, 1707-1719 (2013).

23 Gebrechorkos, S. H., Hülsmann, S. & Bernhofer, C. Regional climate projections for impact assessment studies in East Africa. *Environmental Research Letters* 14, 044031 (2019).

24 Emami, F. & Koch, M. Modeling the impact of climate change on water availability in the Zarrine River Basin and inflow to the Boukan Dam, Iran. *Climate* 7, 51 (2019).

25 Phuong, D. N. D. *et al.* Projections of future climate change in the Vu Gia Thu Bon River Basin, Vietnam by using statistical downscaling model (SDSM). *Water* 12, 755 (2020).

26 Perez, J., Menendez, M., Mendez, F. J. & Losada, I. J. Evaluating the performance of CMIP3 and CMIP5 global climate models over the north-east Atlantic region. *Climate Dynamics* 43, 2663-2680 (2014).

27 Wilby, R. L. & Harris, I. A framework for assessing uncertainties in climate change impacts: Low‐flow scenarios for the River Thames, UK. *Water resources research* 42 (2006).

28 Gleckler, P. J., Taylor, K. E. & Doutriaux, C. Performance metrics for climate models. *Journal of Geophysical Research: Atmospheres* 113 (2008).

29 Aloysius, N. R., Sheffield, J., Saiers, J. E., Li, H. & Wood, E. F. Evaluation of historical and future simulations of precipitation and temperature in central Africa from CMIP5 climate models. *Journal of Geophysical Research: Atmospheres* 121, 130-152 (2016).

30 Wang, R., Cheng, Q., Liu, L., Yan, C. & Huang, G. Multi-model projections of climate change in different RCP scenarios in an arid inland region, Northwest China. *Water* 11, 347 (2019).

31 Kreienkamp, F., Lorenz, P. & Geiger, T. Statistically downscaled CMIP6 projections show stronger warming for Germany. *Atmosphere* 11, 1245 (2020).

32 Chaudhuri, C. & Robertson, C. CliGAN: A structurally sensitive convolutional neural network model for statistical downscaling of precipitation from multi-model ensembles. *Water* 12, 3353 (2020).

33 Knutti, R. Why are climate models reproducing the observed global surface warming so well? *Geophysical Research Letters* 35 (2008).

34 Fenta Mekonnen, D. & Disse, M. Analyzing the future climate change of Upper Blue Nile River basin using statistical downscaling techniques. *Hydrology and Earth System Sciences* 22, 2391-2408 (2018).

35 Hassan, Z., Shamsudin, S. & Harun, S. Application of SDSM and LARS-WG for simulating and downscaling of rainfall and temperature. *Theoretical and applied climatology* 116, 243-257 (2014).

36 Gebrechorkos, S. H., Hülsmann, S. & Bernhofer, C. Evaluation of multiple climate data sources for managing environmental resources in East Africa. *Hydrology and Earth System Sciences* 22, 4547-4564 (2018).

37 Pierce, D. W., Barnett, T. P., Santer, B. D. & Gleckler, P. J. Selecting global climate models for regional climate change studies. *Proceedings of the National Academy of Sciences* 106, 8441-8446 (2009).

38 Raju, K. S. & Kumar, D. N. Ranking of global climate models for India using multicriterion analysis. *Climate research* 60, 103-117 (2014).

39 Zabaleta, A., Meaurio, M., Ruiz, E. & Antigüedad, I. Simulation climate change impact on runoff

and sediment yield in a small watershed in the Basque Country, northern Spain. *Journal of Environmental Quality* 43, 235-245 (2014).

40 Dibike, Y. B. & Coulibaly, P. Hydrologic impact of climate change in the Saguenay watershed: comparison of downscaling methods and hydrologic models. *Journal of hydrology* 307, 145-163 (2005).

41 Jha, P. K. & Minagawa, M. Assessment of denitrification process in lower Ishikari river system, Japan. *Chemosphere* 93, 1726-1733 (2013).

42 Slivinski, L. C. *et al.* Towards a more reliable historical reanalysis: Improvements for version 3 of the Twentieth Century Reanalysis system. *Quarterly Journal of the Royal Meteorological Society* 145, 2876-2908 (2019).

43 Ebi, K. L. *et al.* A new scenario framework for climate change research: background, process, and future directions. *Climatic Change* 122, 363-372 (2014).

44 Van Vuuren, D. P. *et al.* The representative concentration pathways: an overview. *Climatic change* 109, 5-31 (2011).

45 O'Neill, B. C. *et al.* A new scenario framework for climate change research: the concept of shared socioeconomic pathways. *Climatic change* 122, 387-400 (2014).

46 O'Neill, B. C. *et al.* The roads ahead: Narratives for shared socioeconomic pathways describing world futures in the 21st century. *Global environmental change* 42, 169-180 (2017).

47 Riahi, K. *et al.* The Shared Socioeconomic Pathways and their energy, land use, and greenhouse gas emissions implications: An overview. *Global environmental change* 42, 153-168 (2017).

48 Popp, A. *et al.* Land-use futures in the shared socio-economic pathways. *Global Environmental Change* 42, 331-345 (2017).

49 Simpkins, G. Progress in climate modelling. *Nature Climate Change* 7, 684-685 (2017).

50 O'Neill, B. *et al.* The Scenario Model Intercomparison Project (ScenarioMIP) for CMIP6, Geosci. Model Dev., 9, 3461–3482 (2016).

51 Maraun, D. *et al.* Precipitation downscaling under climate change: Recent developments to bridge the gap between dynamical models and the end user. *Reviews of geophysics* 48 (2010).

52 Jain, S., Salunke, P., Mishra, S. K. & Sahany, S. Performance of CMIP5 models in the simulation of Indian summer monsoon. *Theoretical and Applied Climatology* 137, 1429-1447 (2019).

53 Raju, K. S. & Kumar, D. N. Review of approaches for selection and ensembling of GCMs. *Journal of Water and Climate Change* 11, 577-599 (2020).

54 Taylor, K. E. Summarizing multiple aspects of model performance in a single diagram. *Journal of Geophysical Research: Atmospheres* 106, 7183-7192 (2001).

55 Zhang, Y., You, Q., Chen, C. & Ge, J. Impacts of climate change on streamflows under RCP scenarios: A case study in Xin River Basin, China. *Atmospheric Research* 178, 521-534 (2016).

56 Peng, S. *et al.* Response of hydrological processes to climate and land use changes in Hiso River watershed, Fukushima, Japan. *Physics and Chemistry of the Earth, Parts A/B/C* 123, 103010 (2021).

57 Goyal, M. K. & Ojha, C. Downscaling of surface temperature for lake catchment in an arid region in India using linear multiple regression and neural networks. *International Journal of Climatology* 32, 552-566 (2012).